



Room-temperature catalytic oxidation of benzo(a)pyrene by Ce-SBA-15 supported active CeSiO₄ phase

Xuebin Zhang, Shaomin Liu*, Hongwu Tong, Guoping Yong*

Department of Chemistry, University of Science and Technology of China, Hefei 230026, China

ARTICLE INFO

Article history:

Received 11 June 2012

Received in revised form 26 July 2012

Accepted 13 August 2012

Available online 19 August 2012

Keywords:

Ce-SBA-15

CeSiO₄

Benzo(a)pyrene

Room-temperature oxidation

ABSTRACT

A series of cerium-incorporated SBA-15 mesoporous materials were prepared through direct hydrothermal synthesis method, which was characterized by PXRD, N₂ physisorption and TEM measurements. The low-angle PXRD and N₂ physisorption results show the cerium successfully incorporated into the framework of SBA-15. The large angle PXRD results indicate that Ce-SBA-15 mesoporous materials supported CeSiO₄ phase was in situ synthesized by adjusting pH to 6 with anhydrous triethylamine, and then calcined in air at 550 °C. The room-temperature adsorption behaviors of SBA-15 and Ce-SBA-15 materials for benzo(a)pyrene in cyclohexane solutions were investigated. Interestingly, Ce-SBA-15 materials reveal good catalytic performance for room-temperature oxidation benzo(a)pyrene to corresponding quinone through a radical oxidation mechanism, attributable to in situ forming active CeSiO₄ phase which was supported in Ce-SBA-15 material. The benzo(a)pyrene transfer to quinone by CeSiO₄ phase leads to higher adsorption capacity owing to higher affinity of quinone with mesoporous channels, as a result, some Ce-SBA-15 materials exhibit higher adsorption capacity for benzo(a)pyrene than SBA-15 material. The radical oxidation mechanism was demonstrated by EPR and the interception effect of a radical scavenger, TEMPO. The quinone-type molecule was identified by photoluminescence, ESI-MS, IR and NMR.

© 2012 Elsevier B.V. All rights reserved.

1. Introduction

Reducing the emissions of toxic substances such as POPs (persistent organic pollutants) has received special attention for the last 10 years [1]. The POP's family includes polychloro-dibenzodioxins (PCDDs also called dioxins), polychloro-dibenzofurans (PCDFs also called furans), polychlorinated biphenyls (PCBs) and polycyclic aromatic hydrocarbons (PAHs). Their presence in the environment is harmful to humans but also to the ecosystems. In particular, the release of PAHs has started to cause considerable concern. Most PAHs stem from the atmospheric deposition and diesel emission which are mainly emitted during the incomplete combustion of organic matters, such as diesel, gasoline, biomass, coal and wood [2–4]. PAHs are listed as carcinogenic and mutagenic priority pollutants, belonging to the environmental endocrine disrupters. Consequently, the elimination of PAHs is one of the priority and emerging challenges.

A series of different technologies has been developed to reduce PAH emissions including biodegradation, absorption, adsorption, high-energy electron beam, ozonization and catalytic oxidation [5–8]. Among them, catalytic oxidation of PAHs has been

demonstrated to be one of the most promising and cost-effective technologies for the removal of PAHs due to the lower combustion temperatures required and the higher selectivity toward CO₂ [9,10]. Noble metal based catalysts, such as Pt and Pd supported on different metal oxides, are very active for the removal of PAHs, especially naphthalene [11–13]. However, the development of more active and cost-effective catalysts for the complete oxidation of PAHs remains a major research target. Among an extensive range of metal oxide catalysts, it has been demonstrated that CeO₂ were significantly more effective catalysts for the treatment of PAHs emissions, especially naphthalene [14–17], attributable to the Ce³⁺/Ce⁴⁺ redox cycle which leads to high catalytic activity of CeO₂ [5].

Mesoporous SBA-15 has attracted great attention due to its highly ordered hexagonal structure with larger pore diameter, narrow pore size distribution, thick pore wall and high surface areas. However, the pure silica mesoporous SBA-15 has been seldom used as catalyst because of its lack of sufficient acidity and redox properties. The cerium-containing SBA-15 (Ce-SBA-15) materials obtained by the direct hydrothermal method have been reported [18–20]. These cerium-containing SBA-15 materials possessed the typical hexagonal structure of SBA-15, and displayed a large pore diameter and a higher specific surface area than SBA-15 [18]. These cerium-containing SBA-15 materials also show good catalytic activities, such as oxidative of cyclohexane [20], oxidative cleavage of cyclohexene [21]. Moreover, it was found that the mesoporous

* Corresponding authors. Tel.: +86 551 3492147; fax: +86 551 3492065.

E-mail addresses: liusm@ustc.edu.cn (S. Liu), gpyong@ustc.edu.cn (G. Yong).

Ce-SBA-15 supported metal catalysts also exhibit good catalytic performance. The effect of cerium on the activity of Cr-SBA-15 catalyst in oxidative dehydrogenation of ethane to ethylene was investigated [22]. It was found that adding Ce species to Cr/SBA-15 catalysts remarkably changed the redox properties and enhanced the catalytic activity of chromium species in catalysts. Ce-SBA-15 supported cobalt catalyst possesses high catalytic activity in the oxidation of benzene [23]. Zr–Ce-SBA-15 supported palladium catalysts can be used for toluene catalytic oxidation [24]. Ce-SBA-15 supported nickel catalysts exhibit good catalytic performance for methane dry reforming to hydrogen and syngas [25].

Very recently, metal ions incorporating mesoporous materials or mesoporous materials supported metal catalysts showed higher activity for catalytic oxidation of naphthalene [26–30], because mesoporous materials generally exhibit diverse applications, especially catalysis [31–33]. SBA-15 impregnated with CeO₂ was reported to obviously enhance catalytic activity and stability of catalysts for steam reforming of methane, which was due to that CeO₂ layer precoated on SBA-15 [34]. We have discovered that cerium-incorporating mesoporous silica can selective reduction of bulky PAHs from mainstream smoke of cigarettes [35]. In this work, we report the hydrothermal synthesis of cerium-incorporating SBA-15 by co-templating method. It is found that one active phase (CeSiO₄) was in situ formed in Ce-SBA-15 materials. Also, we discover for the first time that adsorbed benzo(a)pyrene (BaP) on Ce-SBA-15 can be oxidized to corresponding quinone at room temperature by active CeSiO₄ phase supported on Ce-SBA-15.

2. Experimental

2.1. Materials and methods

All reagents were commercially available and used without further purification. FT-IR spectrum (KBr disk, 4000–400 cm^{−1}) was recorded on Bruker EQUINOX55 FT-IR spectrophotometer. ¹H and ¹³C NMR spectra were obtained on Bruker Avance 400 MHz NMR spectrometers using CDCl₃ as solvent and tetramethylsilane (TMS) as the internal standard. The powder X-ray diffraction (PXRD) patterns of the samples were collected on a Philips X'Pert PRO SUPER diffractometer operating with nickel-filtered Cu-K α radiation ($\lambda = 1.540598 \text{ \AA}$) at 40 kV and 200 mA. The diffractograms were recorded in the 2θ range of 0.8–10° (low-angle) and 10–70° (wide-angle). Transmission electron microscopy (TEM) images were taken on a JEOL 2010 electron microscope operating at 200 kV. Nitrogen sorption and desorption isotherms were measured at −196 °C with a Micromeritics ASAP 3020 analyzer (Micromeritics, USA). Before measurements, samples were degassed in a vacuum at 200 °C for at least 5 h. The Brunauer–Emmett–Teller (BET) method and the Barrett–Joyner–Halenda (BJH) model were utilized to calculate the specific surface areas (BET), the pore volumes and pore size distributions, respectively. The total pore volumes (V_t) were estimated from the adsorbed branch at a relative pressure P/P_0 of 0.994. The solution photoluminescence (PL) spectra were determined at room temperature on a Fluorolog-3-TAU fluorescence spectrophotometer. The EPR spectra were recorded on a JES-FA 200 ESR spectrometer at X-band. Electrospray ionization mass spectra (ESI-MS) were obtained using a LCQ Advantage Max mass spectrometer (Finnigan, San Jose, CA, USA). The BaP concentrations were analyzed by HPLC-FLD (Agilent 1100) with $\lambda_{\text{ex}} = 297 \text{ nm}$ and $\lambda_{\text{em}} = 405 \text{ nm}$.

2.2. Synthesis of SBA-15 and Ce-SBA-15 materials

In a typical synthesis: 2.7 g of tri-block copolymer pluronic P123 (EO₂₀PO₇₀EO₂₀) was dissolved in 20 mL of H₂O to get a clear solution. Thereafter, 1.683 g of NaCl and 50 mL 0.29 mol/L

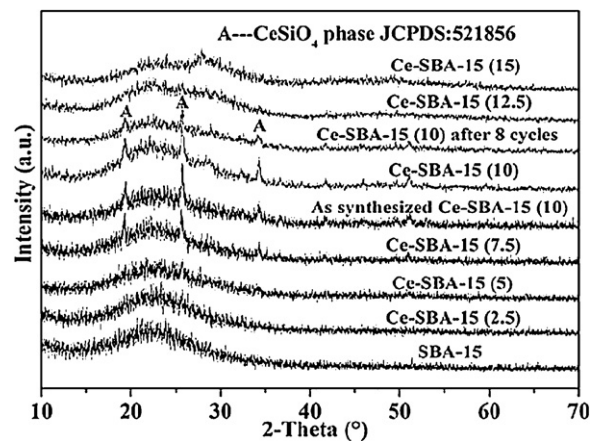


Fig. 1. PXRD patterns at high angle for SBA-15 and Ce-SBA-15 samples.

of HCl were added, and the solution was stirred at 40 °C for 4 h. Then, 5 g of tetraethylorthosilicate (TEOS) and various amounts of Ce(NO₃)₃·6H₂O (the Ce/Si molar ratio of 0, 2.5, 5, 7.5, 10, 12.5 and 15%) were added, and the resulting mixture was stirred at 40 °C for another 20 h. Thereafter, pH value of reaction system was adjusted to 6 using anhydrous triethylamine (TEA), and resulting gel was placed into a Teflon-lined stainless autoclave. The autoclave was sealed and heated at 100 °C for 24 h. The resulting solid was collected by filtration and washed with ethanol, and then dried at 100 °C overnight. Finally, the solid was calcined in air at 550 °C (heating rate 2 °C/min) for 5 h.

2.3. Adsorption of BaP

The adsorption BaP was performed by introducing, under shaking at room temperature for 6 h, 20 mg of the mesoporous material in a 10 mL cyclohexane solution containing different initial concentrations of BaP. Thereafter, the solid was separated by filtration using a 0.45 μm Millex-GVMilli pore filter, and the filtrate was analyzed by HPLC-FLD, in order to calculate adsorption capacity.

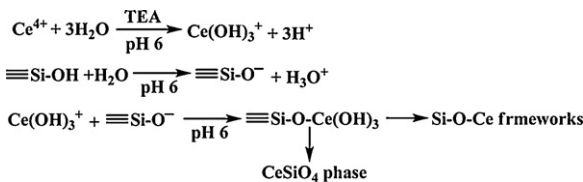
2.4. Extraction of quinone

The in situ forming quinone was eluted by methanol, 100 mg of BaP-adsorbed mesoporous material with 10 mL methanol. Thereafter, the separated solid was finally dried at 150 °C under vacuum condition for recycling experiment. To obtain required amount of quinone, many times experiments were done according to the above process. The combined filtrate was evaporated to dryness under reduced pressure at 50 °C, and then used to carry out PL, IR, ¹H and ¹³C NMR and ESI-MS determination.

3. Results and discussion

3.1. Syntheses

The SBA-15 was prepared according to a procedure described in literature [36]. According to various Ce/Si molar ratios (2.5, 5, 7.5, 10, 12.5 and 15), the synthesized Ce-SBA-15 materials were named as Ce-SBA-15 (2.5), Ce-SBA-15 (5), Ce-SBA-15 (7.5), Ce-SBA-15 (10), Ce-SBA-15 (12.5) and Ce-SBA-15 (15), respectively. Ce(IV) was spontaneously generated from Ce(NO₃)₃·6H₂O during the hydrothermal reactions [37]. The obtained Ce-SBA-15 samples were then scanned for high-angle PXRD patterns to find out whether or not any nanosized CeO₂ phase is present in Ce-containing SBA-15 materials. As shown in Fig. 1, no CeO₂ phase was observed in all Ce-SBA-15 samples. Unexpectedly, the CeSiO₄

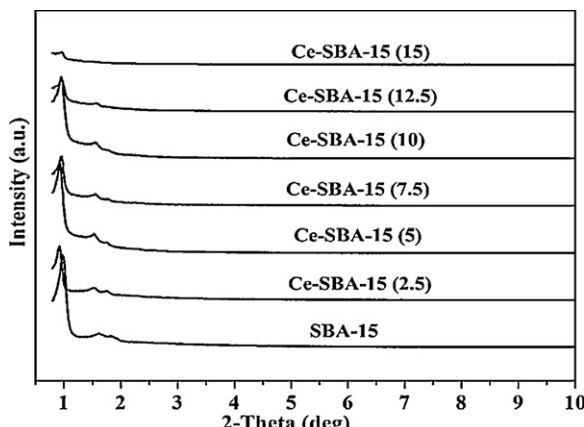
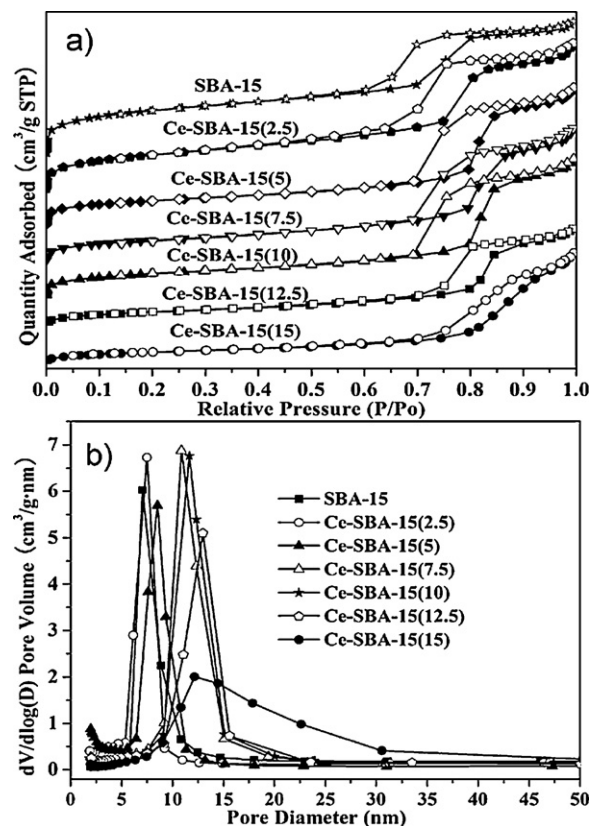
**Scheme 1.** Possible process of in situ formation of CeSiO₄ phase.

phase is observed both in as-synthesized and calcined samples. It is noticeable that when Ce/Si molar ratios increase from 2.5% to 10%, the diffraction intensity of CeSiO₄ phase in the corresponding Ce-SBA-15 samples is enhanced. However, when Ce/Si molar ratios are further increased to 12.5%, the diffraction pattern of CeSiO₄ phase disappeared (Fig. 1).

Generally, the mesoporous Ce-SBA-15 materials synthesized under strong acidic condition (pH < 1) have low amounts of cerium incorporated into SBA-15 [20]. However, lowering the acidity of the solution may decrease the hydrolysis rate of the cerium precursor to match that of the silicon precursor. This might enhance the interaction between the Ce-OH and Si-OH species in the synthesis gel. When decreasing H⁺ concentration in the synthesis gel, the concentration of cerium hydroxyl species increases. Hence, under lesser concentration of H⁺ in the synthesis gel at pH > 2, the structural and textural order of the mesoporous framework are also still maintained. Moreover, CeSiO₄ phase could only be formed in acidic media and more readily produced at higher temperatures [37], the weak acidic condition (pH 6) in reaction system which was adjusted with weak base (TEA) is helpful to forming CeSiO₄ phase. We think weak acidic condition not only synthesizes ordered mesoporous Ce-SBA-15, but leads to in situ formation of CeSiO₄ phase as well, as suggested process in Scheme 1. CeSiO₄ was confirmed to be a zircon-type structure with space group *I41/amd* and unit cell parameters: *a* = 6.9564(3), *c* = 6.1953(4) Å, as reported by Glasser [37,38].

3.2. Characterization of the Ce-SBA-15 samples

For low cerium-incorporated samples, the calcined Ce-SBA-15 materials retain its hexagonally packed porous structure as shown in the small angle PXRD patterns (Fig. 2). From the low-angle PXRD patterns, three peaks can be observed with the strongest one corresponding to (100) diffraction, together with two well-resolved (110) and (200) peaks. This suggested that these Ce-SBA-15 materials have highly ordered 2D hexagonal mesoporous structure (p6mm) and the introduction of cerium does not destroy the mesoporous structure of SBA-15 [39]. Conversely, for

**Fig. 2.** Small angle PXRD patterns of SBA-15 and Ce-SBA-15 samples.**Fig. 3.** (a) Nitrogen adsorption/desorption isotherms and (b) pore-size distribution curves of SBA-15 and Ce-SBA-15 samples.

higher cerium-incorporated samples (Ce/Si molar ratio > 12.5%), the intensity of (100) diffraction becomes very weak, and (110) and (200) peaks essentially disappeared, implying ordered mesoporous structure is significantly destroyed for these samples. Moreover, after incorporating cerium, the (100) peak is shifted to lower 2θ values (Fig. 2). It can be explained by the distinction of atomic radius of Ce⁴⁺ (1.06 Å) and Si⁴⁺ (0.39 Å). Considering the Ce–O bond length is longer than that of Si–O, it can be speculated that cerium species has been incorporated into the mesoporous framework of SBA-15 [40].

As shown in Fig. 3, SBA-15 and Ce-SBA-15 exhibit similar N₂ adsorption/desorption isotherms of IV-type with an H1-type hysteresis loop of mesoporous materials. The profiles are the characteristic of mesoporous materials having cylindrical channels. Three well-distinguished regions of the adsorption isotherms (Fig. 3a) are obvious: (1) monolayer multilayer adsorption ($P/P_0 = 0\text{--}0.5$); (2) capillary condensation ($P/P_0 = 0.5\text{--}0.8$) and (3) multilayer adsorption on the outer surface ($P/P_0 = 0.8\text{--}1.0$). A sharp inflection in the relative pressure (P/P_0) between 0.5 and 0.8 corresponds to capillary condensation within uniform mesopores, and is a function of the pore diameter. The uniform pore size distribution is demonstrated by the sharpness of this step and displayed in the insets of Fig. 3b. However, Ce-SBA-15 (15) shows a wider pore size distribution, corresponding to its disordered mesoporous structure as demonstrated by PXRD pattern. The SBA-15 has a large BET surface area of 843.6 m²/g, high pore volume of 1.15 cm³/g, and moderate pore size of 6.3 nm, but Ce-SBA-15 materials possess lower BET surface area (Table 1). Interestingly, the BET surface area of the Ce-SBA-15 materials exhibits gradual decrease, when increasing the cerium content in materials (Table 1). Ce-SBA-15 materials also possess obviously large pore size compared with SBA-15 (Table 1). The larger pore size of Ce-SBA-15 materials after

Table 1

The physical-chemical properties of SBA-15 and Ce-SBA-15 samples.

Materials	S_{BET}^a (m ² /g)	V_p^b (cm ³ /g)	D_p^b (nm)
SBA-15	843.6	1.15	6.26
Ce-SBA-15 (2.5)	690.8	1.27	7.36
Ce-SBA-15 (5)	471.6	1.20	9.73
Ce-SBA-15 (7.5)	436.7	1.19	10.44
Ce-SBA-15 (10)	415.4	1.15	11.07
Ce-SBA-15 (12.5)	388.3	0.93	12.31
Ce-SBA-15 (15)	295.9	0.89	13.82

^a The specific surface area was calculated by using the BET (Brunauer–Emmett–Teller) model.

^b The pore volume and pore size distributions were determined by the BJH (Barrett–Joyner–Halenda) method.

Ce(IV) functionalization should be attributed to the longer Ce–O bond length, because the atomic radius of Ce⁴⁺ (1.06 Å) is larger than that of Si⁴⁺ (0.39 Å). Low BET surface area of Ce-SBA-15 suggests CeSiO₄ phase has highly filled in the mesoporous channels, which partly blocks the pore space of mesoporous channels [41].

The morphology of Ce-SBA-15 is depicted in Fig. 4. The TEM image displays that the mesoporous structure was retained for Ce-SBA-15 (10) sample. One can also observe the dark CeSiO₄ phase supported on Ce-SBA-15 (10) sample from TEM micrograph (Fig. 4a). The pale yellow solid of Ce-SBA-15 sample also demonstrates the existence of CeSiO₄ phase, because CeSiO₄ itself is a pale yellow solid [37]. The HRTEM pattern of CeSiO₄ phase in Ce-SBA-15 (10) is shown in Fig. 4b, which further supports

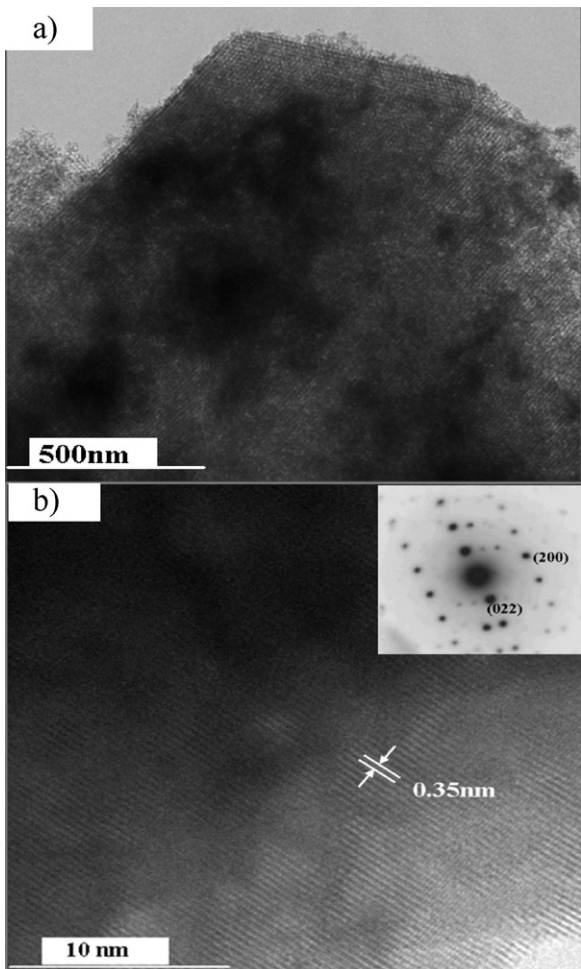


Fig. 4. TEM (a) and HRTEM (b) image of Ce-SBA-15 (10). The inset in (b) is the SAED of Ce-SBA-15 (10).

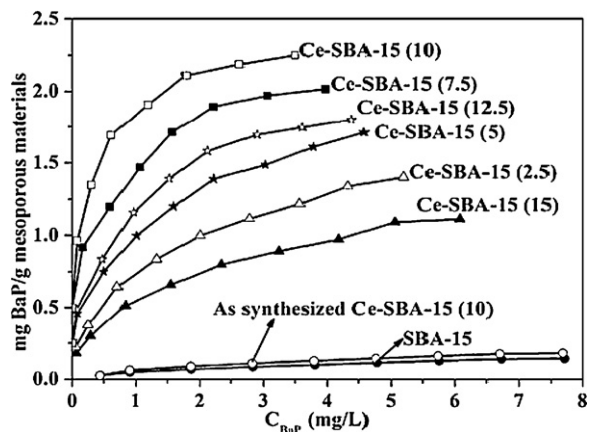


Fig. 5. Adsorption curves of SBA-15 and Ce-SBA-15 mesoporous materials for BaP cyclohexane solutions at room temperature.

the single-crystalline nature of the particles. The interlayer distance was calculated to be \approx 0.35 nm, which agrees well with the separation between the (200) lattice planes. The EDX spectrum (Fig. S1, in Supporting Information) indicates Ce-SBA-15 (10) sample is composed of Ce, O and Si elements.

3.3. The adsorption behavior of SBA-15 and Ce-SBA-15 materials for BaP

Initially, the room-temperature adsorption behavior of SBA-15 and Ce-SBA-15 materials for BaP solution in cyclohexane was investigated. It is obviously found that when Ce/Si molar ratios increase from 0% to 10%, the adsorption capacity of Ce-SBA-15 materials for BaP tends to increase (Fig. 5), however, when Ce/Si molar ratios are further increased to 12.5% and 15%, the BaP adsorption capacities on these two materials decreased (Fig. 5). Particularly, Ce-SBA-15 (15) sample exhibits low adsorption capacity for BaP. Regardless of large surface area and moderate pore size, SBA-15 exhibits very low adsorption capacity for BaP. These experimental results indicate the adsorption interactions of SBA-15 and Ce-SBA-15 materials for BaP can not be attributed to the surface area or shape selectivity effects of these mesoporous materials, because the materials (from Ce-SBA-15 (2.5) to Ce-SBA-15 (10)) with low surface area show higher adsorption capacities than that SBA-15 itself with high surface area (Table 1). Furthermore, compared to Ce-SBA-15 materials, SBA-15 should possess good shape selectivity for BaP due to its small pore size (Table 1), but it exhibits very low adsorption capacity. Kuehl suggests that pore size should be large enough to allow PAHs diffusion along the mesoporous channels; nevertheless, it should also be small enough to provide a potential field that retains adsorbed molecules for shape selectivity [42]. Consequently, the adsorption interactions cannot effectively interpret higher adsorption capacities of some Ce-SBA-15 materials (from Ce-SBA-15 (2.5) to Ce-SBA-15 (12.5)), it must have other reason.

3.4. Room-temperature catalytic oxidation of benzo(a)pyrene

When using Ce-SBA-15 (10) as adsorbent due to its highest adsorption capacity, an unexpected phenomenon was observed in the adsorption experiment: the adsorption system was gradually changed to orange and even red color during a short adsorption period at room temperature. According that adsorption equilibrium can be rapidly reached (achieving saturation adsorption with about 1 h) when using Ce-SBA-15 (10) as adsorbent (Fig. 6), the images of equilibrium systems with different initial BaP concentrations are taken at room temperature (Fig. 7a). One can see that colors of the different equilibrium systems are gradually changed to orange

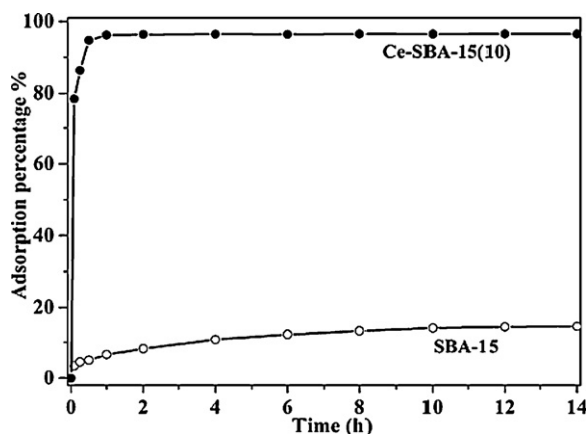
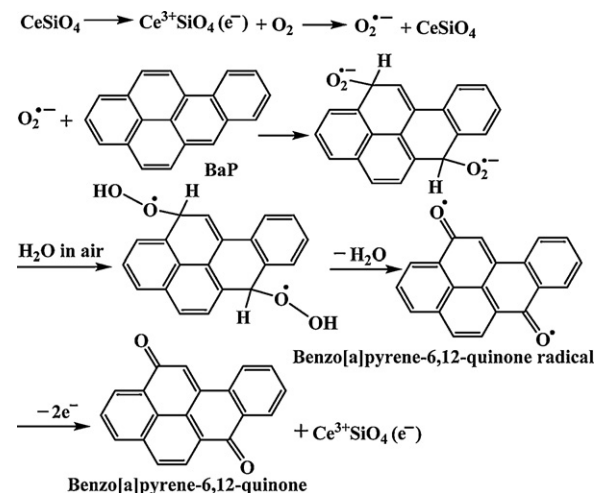


Fig. 6. Adsorption kinetics of BaP cyclohexane solutions ($C_0 = 3$ mg/L) on SBA-15 and Ce-SBA-15 (10) mesoporous materials at room temperature.

and even red with increasing initial BaP concentrations. Such color changes should be attributed to BaP transferring to corresponding quinone through catalytic oxidation by active CeSiO_4 phase. Actually, BaP can be oxidized to quinone by cerium salt [43]. This transfer reaction is probably radical oxidation mechanism by in situ forming $\text{O}_2^{\bullet-}$ under air condition at room temperature (**Scheme 2**). A control experiment with Ce-SBA-15 (10), BaP solution in cyclohexane and a radical scavenger (TEMPO) was carried out, the result shows the catalytic oxidation reaction was completely shut off (**Fig. 8**), because no red equilibrium system was observed when using TEMPO as a radical scavenger. This result indicates that the reaction involved radical intermediates as shown in **Scheme 2**.

Red equilibrium systems should derive from the formation of quinone. When BaP was transferred to corresponding quinone, molecular dipole was increased. As a result, quinone reveals higher affinity with mesoporous channels of Ce-SBA-15 (10), which further promotes BaP to be adsorbed and then to be transferred to quinone, giving rise to much higher adsorption capacities than that of SBA-15. On the other hand, when Ce/Si molar ratios exceed 12.5%, the corresponding material (Ce-SBA-15 (15)) exhibits low adsorption capacity, because there is no observed CeSiO_4 phase in this material, consequently, it cannot effectively transfer BaP to quinone, leading to low adsorption capacity. The Ce-SBA-15 (15) sample still exhibits slightly higher adsorption capacity than that of SBA-15, attributable to low concentration CeO_2 nanoparticles in



Scheme 2. Proposed mechanism for room-temperature catalytic oxidation BaP to benzo(a) pyrene-6,12-quinone by active CeSiO_4 .

the Ce-SBA-15 (15) sample, although these CeO_2 nanoparticles cannot be observed by PXRD. Although the as-synthesized Ce-SBA-15 (10) also contains CeSiO_4 phase, it still exhibits very low adsorption capacity for BaP, because P123 templates occupy the channels that impede the adsorption of BaP. From above experimental results, we think Ce-SBA-15 materials, such as Ce-SBA-15 (7.5) and Ce-SBA-15 (10), first adsorb BaP, the adsorbed-BaP then is transferred to quinone, resulting in higher adsorption capacities. Among, catalytic oxidation by active CeSiO_4 phase is a key factor to increase BaP adsorption capacities. Conversely, the materials without CeSiO_4 phase (SBA-15 and SBA-15 (15)) reveal very low adsorption capacities for BaP which support catalytic oxidation by active CeSiO_4 phase is a key factor; the as-synthesized Ce-SBA-15 (10) material that contains CeSiO_4 phase, but possesses very small channels also exhibits very low adsorption capacity (**Fig. 5**) indicate the adsorption is initial process. In addition, the color changing extent of adsorption equilibrium systems with various materials is relative to content of CeSiO_4 phase in the materials (**Fig. S2**). Because methanol has high affinity with quinone, Ce-SBA-15 (10) material offer ease of handling and purification through simple extraction of quinone by methanol (**Fig. S3**), giving rise to its recovery and recycling. In order to examine this possibility, we carried out adsorption and



Fig. 7. Photographs of equilibrium systems of Ce-SBA-15 (10) with (a) different initial BaP concentrations and (b) initial BaP concentration of 9 mg/L for 6 recycling experiments. (For interpretation of the references to color in this figure legend, the reader is referred to the web version of the article.)



Fig. 8. Photographs of equilibrium systems of Ce-SBA-15 (10) without TEMPO (left) and with TEMPO (right). (For interpretation of the references to color in this figure legend, the reader is referred to the web version of the article.)

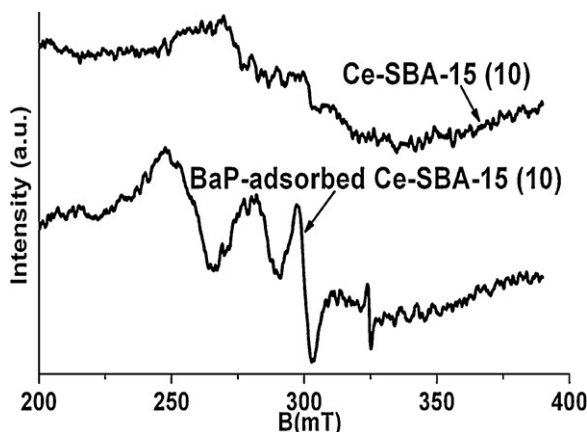


Fig. 9. Solid-state EPR spectra of Ce-SBA-15 (10) and BaP-adsorbed Ce-SBA-15 (10) at room temperature (BaP-adsorbed Ce-SBA-15 (10) was separated from equilibrium system by filtration, washed with water and dried at 40 °C).

in situ catalytic oxidation reaction for 8 times with the same Ce-SBA-15 (10) material under the same condition. Before reuse, the quinone was extracted by methanol from BaP-adsorbed Ce-SBA-15 (10), the solid was separated by filtration, washed with methanol and finally dried at 150 °C under vacuum condition. The similar colors (Fig. 7b) of equilibrium systems for 8 cycles and the almost the same PXRD pattern of CeSiO₄ in Ce-SBA-15 (10) after reused 8 times indicate that Ce-SBA-15 (10) can be repeatedly used more than 8 times without apparently decreasing catalytic activity of CeSiO₄.

The in situ forming quinone was further demonstrated by EPR, photoluminescence (PL), ESI-MS, IR and NMR. The solid-state EPR spectra were recorded for Ce-SBA-15 (10) and BaP-adsorbed Ce-SBA-15 (10) at room temperature (Fig. 9). No EPR signal for Ce-SBA-15 (10) is observed, however, BaP-adsorbed Ce-SBA-15 (10) exhibits two isotropic EPR signals centered at $g=2.14$ and 2.00, corresponding to Ce³⁺ and quinone radical, respectively. The EPR results demonstrate radical oxidation mechanism as proposed above. Moreover, methanol extraction solution was EPR silent, implying it mainly exists as quinone, or quinone radical exists as diamagnetic ($S=0$) π -dimer [44]. On the other hand, when using TEMPO as a radical scavenger, such BaP-adsorbed Ce-SBA-15 (10) exhibits a symmetrical resonance EPR signal with g -value of 1.998 (Fig. S4), indicating a typical organic radical of TEMPO. Compared to PL spectrum of BaP in cyclohexane solution (Fig. S5), PL spectra of methanol extraction solutions with different initial BaP concentrations exhibit a new characteristic emission band at about 556 nm (Fig. 10), which are presumably ascribed to quinone-type molecule.

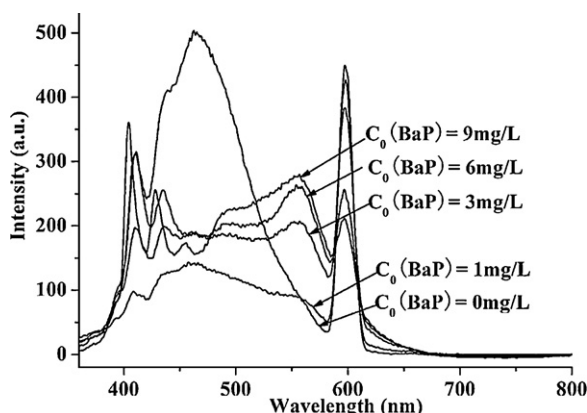


Fig. 10. Room-temperature PL spectra of methanol extraction solutions from BaP-adsorbed Ce-SBA-15 (10) with different initial BaP concentrations.

The quinone-type molecule in methanol extraction solution was also judged from IR (Fig. S6), ESI-MS (Fig. S7), and ¹H and ¹³C NMR (Figs. S8 and S9). The IR absorption band of methanol extraction solution at about 1729 cm⁻¹ (marked by asterisk) is assigned to the stretching vibration of quinone carbonyl group. Even if it is difficult to obtain purified quinone-type molecule from methanol extraction solution, ¹³C NMR displays signals with δ values between 180 and 185 ppm, also indicative of the presence of quinone carbonyl group.

4. Conclusion

In conclusion, we have discovered an active CeSiO₄ phase which was in situ formed during synthesis of Ce-SBA-15 mesoporous materials. Interestingly, at room temperature, BaP can be transferred to corresponding quinone catalyzed by this active CeSiO₄ phase through a radical oxidation mechanism. Such catalytic oxidation reaction also results in high adsorption capacities for BaP on Ce-SBA-15 materials. The catalytic oxidation BaP at room temperature makes such mesoporous materials promising candidates for potential applications in reducing the emissions of toxic BaP. The further extension of this work to reducing other PAHs is in progress.

Acknowledgment

We gratefully acknowledge the National Nature Science Foundation of China (21172210) for financial support.

Appendix A. Supplementary data

Supplementary data associated with this article can be found, in the online version, at <http://dx.doi.org/10.1016/j.apcatb.2012.08.008>.

References

- [1] K. Breivik, R. Alcock, Y.F. Li, R.E. Bailey, H. Fiedler, J.M. Pacyna, Environmental Pollution 128 (2004) 3–16.
- [2] B.J. Finlayson-Pitts, J.N. Pitts Jr., Chemistry of the Upper and Lower Atmosphere, first ed., Academic Press, San Diego, 1999, p. 436.
- [3] A.M. Mastral, M.S. Callen, T. Garcia, Energy Fuels 14 (2000) 164–168.
- [4] P.J. Li, X.J. Li, F. Stagnitti, H.R. Zhang, X. Lin, S.Y. Zang, J.C. Zhuo, X.Z. Xiong, Journal of Hazardous Materials 162 (2009) 463–468.
- [5] P.H. McMurry, Atmospheric Environment 34 (2000) 1959–1999.
- [6] G. Chen, K.A. Strevett, B.A. Vanegas, Biodegradation 12 (2001) 433–442.
- [7] N.E. Ntaijua, S.H. Taylor, Topics in Catalysis 52 (2009) 528–541.
- [8] P. Laveille, A. Falcimaigne, F. Chamouleau, G. Renard, J. Drone, F. Fajula, S. Pulvin, D. Thomas, C. Bailly, A. Galarneau, New Journal of Chemistry 34 (2010) 2153–2165.
- [9] S.O. Baek, R.A. Field, M.E. Goldstone, P.W. Kirk, J.N. Lester, Water, Air, and Soil Pollution 60 (1991) 279–300.
- [10] S. Scirè, S. Minicò, C. Crisafulli, C. Satriano, A. Pistone, Applied Catalysis B: Environmental 40 (2003) 43–49.
- [11] X.W. Zhang, S.C. Shen, L.E. Yu, S. Kawi, K. Hidajat, K.Y. Simon Ng., Applied Catalysis A: General 250 (2003) 341–352.
- [12] X.W. Zhang, S.C. Shen, K. Hidajat, S. Kawi, L.E. Yu, K.Y. Simon Ng., Catalysis Letters 96 (2004) 87–96.
- [13] E. Ntaijua N., A.F. Carley, S.H. Taylor, Catalysis Today 137 (2008) 362–366.
- [14] T. Garcia, B. Solsona, S.H. Taylor, Catalysis Letters 105 (2005) 183–189.
- [15] T. Garcia, B. Solsona, S.H. Taylor, Applied Catalysis B: Environmental 66 (2006) 92–99.
- [16] A. Aranda, J.M. López, R. Murillo, A.M. Mastral, A. Dejoz, I. Vázquez, B. Solsona, S.H. Taylor, T. García, Journal of Hazardous Materials 171 (2009) 393–399.
- [17] B. Puertolas, B. Solsona, S. Agouram, R. Murillo, A.M. Mastral, A. Aranda, S.H. Taylor, T. García, Applied Catalysis B: Environmental 93 (2010) 395–405.
- [18] M.N. Timofeeva, S.H. Jhung, Y.K. Hwang, D.K. Kim, V.N. Panchenko, M.S. Melgunov, Yu.A. Chesarov, J.S. Chang, Applied Catalysis A: General 317 (2007) 1–10.
- [19] Q.G. Dai, X.Y. Wang, G.P. Chen, Y. Zheng, G.Z. Lu, Microporous and Mesoporous Materials 100 (2007) 268–275.
- [20] M. Selvaraj, D.W. Park, C.S. Ha, Microporous and Mesoporous Materials 138 (2011) 94–101.
- [21] M.N. Timofeeva, O.A. Kholdeeva, S.H. Jhung, J.S. Chang, Applied Catalysis A: General 345 (2008) 195–200.
- [22] X.J. Shi, S.F. Ji, K. Wang, Catalysis Letters 125 (2008) 331–339.

[23] Z. Mu, J.J. Li, H. Tian, Z.P. Hao, S.Z. Qiao, *Materials Research Bulletin* 43 (2008) 2599–2606.

[24] F. Wang, J.S. Li, J.F. Yuan, X.Y. Sun, J.Y. Shen, W.Q. Han, L. Wang, *Catalysis Communications* 12 (2011) 1415–1419.

[25] N. Wang, W. Chu, T. Zhang, X.S. Zhao, *International Journal of Hydrogen Energy* 37 (2012) 19–30.

[26] S.C. Marie-Rose, T. Belin, J. Mijoin, E. Fiani, M. Taralunga, F. Nicol, X. Chaucherie, P. Magnoux, *Applied Catalysis B: Environmental* 90 (2009) 489–496.

[27] J.I. Park, J.K. Lee, J. Miyawaki, W.W. Pang, S.H. Yoon, I. Mochida, *Catalysis Communications* 11 (2010) 1068–1071.

[28] J.I. Park, J.K. Lee, J. Miyawaki, S.H. Yoon, I. Mochida, *Journal of Industrial and Engineering Chemistry* 17 (2011) 271–276.

[29] N. Narendra, K. Suresh Kumar Reddy, K.V.V. Krishna Mohan, S.J. Kulkarni, A. Koekritz, K.V. Raghavan, *Journal of Porous Materials* 18 (2011) 337–343.

[30] A. Aranda, E. Aylon, B. Solsona, R. Murillo, A.M. Mastral, D.R. Sellick, S.T. Agouram, T. Garcia, S.H. Taylor, *Chemical Communications* 48 (2012) 4704–4706.

[31] Y. Zhou, J. Yang, J.Y. Yang, F.N. Gu, Y. Wang, J.H. Zhu, *Journal of Materials Chemistry* 21 (2011) 13895–13901.

[32] D. Tian, G.P. Yong, Y. Dai, X.Y. Yan, S.M. Liu, *Catalysis Letters* 130 (2009) 211–216.

[33] G.P. Yong, D. Tian, H.W. Tong, S.M. Liu, *Journal of Molecular Catalysis A: Chemical* 323 (2010) 40–44.

[34] K. Wang, X.J. Li, S.F. Ji, X.J. Shi, J.J. Tang, *Energy Fuels* 23 (2009) 25–31.

[35] G.P. Yong, Z.X. Jin, H.W. Tong, X.Y. Yan, G.S. Li, S.M. Liu, *Microporous and Mesoporous Materials* 91 (2006) 238–243.

[36] Y.J. Han, J.M. Kim, G.D. Stucky, *Chemistry of Materials* 12 (2000) 2068–2069.

[37] C.L. Dickson, F.P. Glasser, *Cement and Concrete Research* 30 (2000) 1619–1623.

[38] J.M.S. Skakle, C.L. Dickson, F.P. Glasser, *Powder Diffraction* 15 (2000) 234–238.

[39] S.Y. Chen, J.F. Lee, S. Cheng, *Journal of Catalysis* 270 (2010) 196–205.

[40] S.C. Laha, P. Mukherjee, S.R. Sainkar, R. Kumar, *Journal of Catalysis* 207 (2002) 213–223.

[41] X.G. Zhao, J.L. Shi, B. Hu, L.X. Zhang, Z.L. Hua, *Materials Letters* 58 (2004) 2152–2156.

[42] G.H. Kuehl, US Patent No. 5 583 277 (1996).

[43] G. Balanikas, N. Hussain, S. Amin, S.S. Hecht, *Journal of Organic Chemistry* 53 (1988) 1007–1010.

[44] G.P. Yong, C.F. Li, Y.Z. Li, S.W. Luo, *Chemical Communications* 46 (2010) 3194–3196.